



Degradation of SERRATE via ubiquitin-independent 20S proteasome to survey RNA metabolism

Yanjun Li[®]^{1,2,3,8}, Di Sun[®]^{1,2,8}, Zeyang Ma^{1,2}, Karissa Yamaguchi[®]¹, Lin Wang^{1,2,3}, Songxiao Zhong[®]^{1,2}, Xingxing Yan^{1,2}, Baoshuan Shang^{1,2}, Yukihiro Nagashima⁴, Hisashi Koiwa⁴, Jiajia Han[®]^{5,6}, Qi Xie[®]⁵, Mingguo Zhou³, Zhiye Wang[®]^{1,2,7} and Xiuren Zhang[®]^{1,2}

SERRATE (SE) is a key factor in RNA metabolism. Here, we report that SE binds 20S core proteasome α subunit G1 (PAG1) among other components and is accumulated in their mutants. Purified PAG1-containing 20S proteasome degrades recombinant SE via an ATP- and ubiquitin-independent manner in vitro. Nevertheless, *PAG1* is a positive regulator for *SE* in vivo, as *pag1* shows comparable molecular and/or developmental defects relative to se. Furthermore, SE is poorly assembled into macromolecular complexes, exemplified by the microprocessor in *pag1* compared with Col-O. *SE* overexpression triggered the destruction of both transgenic and endogenous protein, leading to similar phenotypes of *se* and *SE* overexpression lines. We therefore propose that PAG1 degrades the intrinsically disordered portion of SE to secure the functionality of folded SE that is assembled and protected in macromolecular complexes. This study provides insight into how the 20S proteasome regulates RNA metabolism through controlling its key factor in eukaryotes.

ellular signalling and processes can be influenced by protein accumulation levels. The majority of cellular proteins are degraded through a ubiquitin-dependent 26S proteasome pathway in mammalian cells1 and similarly in plants2. In a canonical pathway, ubiquitin, a 76-amino-acid-residue protein, is covalently conjugated through coordinate activities of E1, E2 and E3 enzymes to substrates, marking them for degradation by 26S proteasomes. The 26S proteasome is made up of two subparticles: one or two terminal 19S regulatory particles, which serve as a proteasome activator; and 20S core proteasome, which executes the degradation process^{3–5}. In Arabidopsis, 20S core proteasome contains seven α subunits and seven β subunits, which are assembled in a $\alpha_{1-7}/\beta_{1-7}/\beta_{1-7}/\alpha_{1-7}$ configuration⁶. Increasing evidence has shown that intrinsically disordered proteins (IDPs), exemplified by p53 and p21 in animals, contain unstructured regions and are inherently unstable. Such proteins are susceptible to ubiquitin-independent degradation via core 20S proteasomes alone⁷. Of note, many IDPs may also contain certain parts that are folded. In these scenarios, the 19S regulatory subunits can unfold the folded domains of the IDPs and promote their destruction. The IDPs can thus be subjected to both degradation pathways in certain circumstances^{8,9}. Whether there are IDPs and how they are destroyed in plants have not been sufficiently studied.

SERRATE (SE) is a multifunctional protein. SE was initially known as a founding member of the plant microprocessor, acting with DCL1 and HYL1 to produce microRNAs (miRNAs)^{10,11}. Whereas some argue for a direct role for SE in promoting the enzymatic activity and accuracy of DCL1 (refs. ^{12,13}), recent studies propose that SE might act as a scaffold to recruit the processing machinery (including DCL1/HYL1) to proper RNA substrates, or vice versa, to produce miRNAs in vivo^{14–16}. SE also recruits auxiliary

factors such as CHR2/BRM to the microprocessor to fine-tune primary miRNA (pri-miRNA) processing to maintain homeostasis of miRNA production¹⁷. Similarly, the mammalian orthologue of SE, Arsenic resistance protein 2 (Ars2)18,19 participates in miRNA- and short-interfering-RNA-dependent silencing, suggesting the conserved function of SE/Ars2 in RNA silencing throughout eukaryotes^{18,19}. SE and Ars2 also contribute to other aspects of RNA metabolism-for instance, splicing of precursor messenger RNA (pre-mRNA) (especially in the processing of the first introns and 3' end formation), biogenesis of non-coding RNAs, RNA transport and RNA stability^{20–24}. Some of these functions are fulfilled presumably through the interaction with nuclear cap-binding complex (CBC), which consists of two subunits (CBP20 and CBP80) and binds to m⁷G-caps at the 5' ends of polymerase II (pol II)-produced transcripts^{20,23,24}. In addition, SE acts as a transcriptional factor, regulating the expression of transposons²⁵ and intronless protein-coding genes²⁶. SE does so either through partnering with histone 3 lysine 27 monomethylation (H3K27me1) methyltransferases ATXR5 and ATXR6 (ref. 25) or through interplaying with RNA polymerase II (ref. ²⁶). In mammals, Ars2 also activates the transcription of SOX2, a gene involved in stem cell maintenance27. Despite the critical roles of SE/Ars2 in RNA metabolism, little is known about how the proteins themselves are regulated. A recent structural analysis of SE/Ars2 revealed that only the middle parts of the proteins could be crystallized whereas large portions are unstructured²⁸, suggesting that SE/ Ars2 might be IDPs, and subject to degradation via 20S proteasome.

Results

Knockdown mutants of *PAG1* display pleiotropic developmental defects. We identified a bona fide partner of SE, PAG1

¹Department of Biochemistry and Biophysics, Texas A&M University, College Station, TX, USA. ²Institute for Plant Genomics and Biotechnology, Texas A&M University, College Station, TX, USA. ³College of Plant Protection, Nanjing Agricultural University, Nanjing, China. ⁴Department of Horticultural Sciences, Texas A&M University, College Station, TX, USA. ⁵State Key Laboratory of Plant Genomics, Institute of Genetics and Developmental Biology, The Innovative Academy of Seed Design, Chinese Academy of Sciences, Beijing, China. ⁶Yunnan Key Laboratory of Plant Reproductive Adaption and Evolutionary Ecology, Yunnan University, Kunming, China. ⁷State Key Laboratory of Plant Physiology and Biochemistry, College of Life Sciences, Zhejiang University, Hangzhou, China. ⁸These authors contributed equally: Yanjun Li, Di Sun. [∞]e-mail: wangzhiye1@zju.edu.cn; xiuren.zhang@tamu.edu

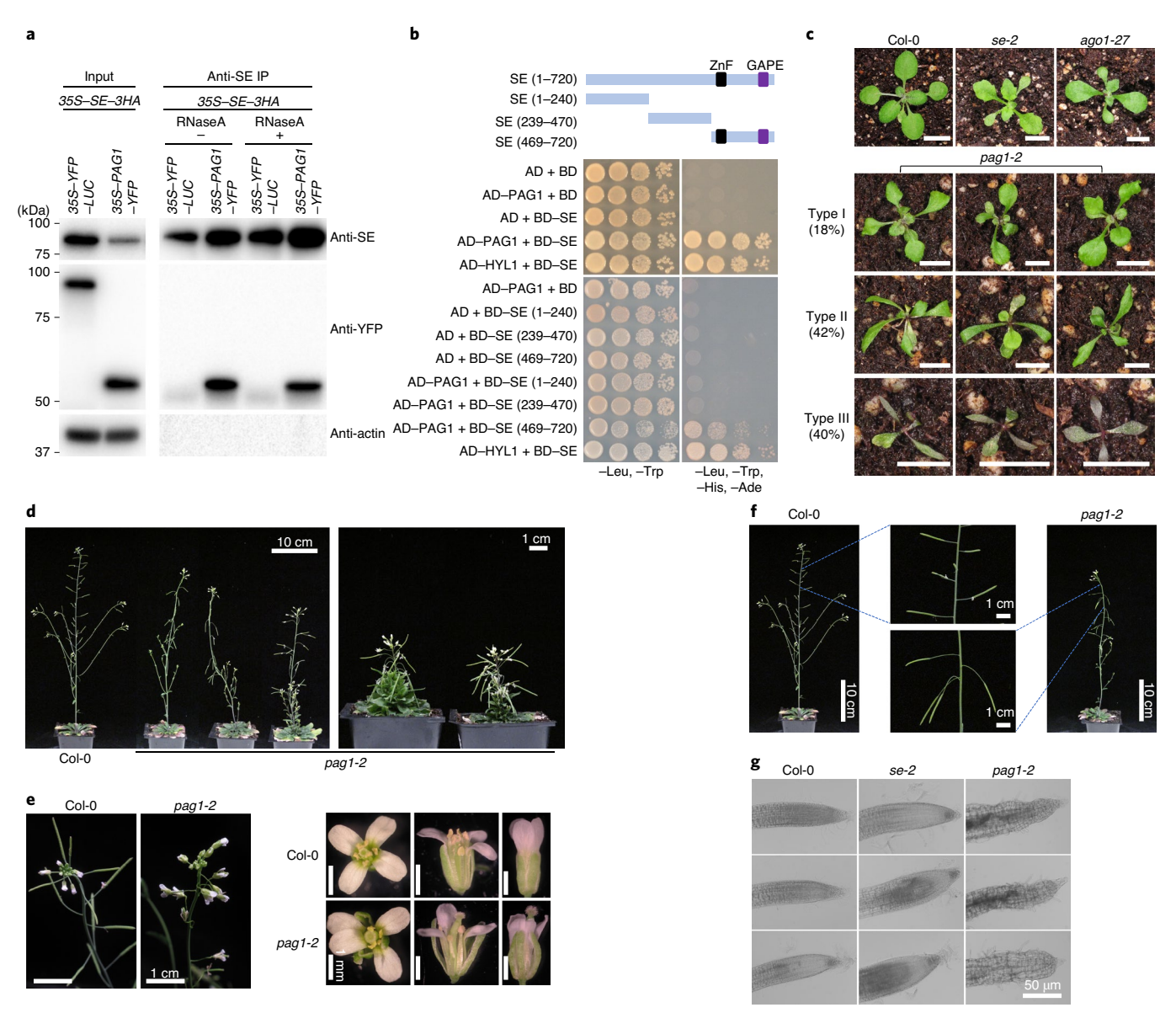


Fig. 1 | Knockdown mutants of PAG1, a partner of SE, cause developmental defects in *Arabidopsis.* **a,b**, The specific SE-PAG1 interaction was confirmed by co-immunoprecipitation (Co-IP) (**a**) and Y2H assays (**b**). In **a**, the constructs harbouring *35S-PAG1-YFP* and *35S-YFP-LUC* were co-infiltrated with *35S-SE-3HA* in *Nicotiana benthamiana*. IP was conducted by a SE-specific antibody. A western blot analysis was done using anti-SE, -YFP or -actin antibodies to detect the indicated proteins in the input and IP products. YFP-LUC and actin serve as negative controls. The experiment was independently repeated three times with similar results. In **b**, a schematic illustration of the full-length and truncated variants of SE used for Y2H is shown. ZnF, zinc finger domain; GAPE, a conserved region enriching Gly, Ala, Pro, Glu residues; AD, GAL4 activation domain; AD-PAG1/HYL1, PAG1/HYL1 fused with AD; BD, GAL4 DNA binding domain; BD-SE, SE fused with BD. The positive control is AD-HYL1+BD-SE; the negative control is AD/BD vectors. At least 15 independent colonies for each combination were tested and showed similar results. **c**, Leaf morphology of 21-d-old *pag1-2* transgenic lines and selected mutants in the miRNA pathway. Scale bars, 0.5 cm. The percentages were calculated from 400 transgenic lines. **d**, Statues of adult plants of Col-O and various hypomorphic *pag1-2* mutants. **e**, Flower developmental defects in *pag1-2*. **f**, Siliques from the hypomorphic *pag1-2* display an upside-down phenotype. **g**, Enlarged and deformed cells in the root tips of *pag1-2* and se-2. In **d-g**, at least ten independent transgenic lines were photographed, and representative images are shown.

protein (AT2G27020), an α subunit of 20S proteasome, and determined that PAG1 interacts with the C-terminal part of SE (469–720 amino acids), the same domain where CHR2 (ref. ¹⁷) or ATXR5 (ref. ²⁵) interacts (Fig. 1a,b, Extended Data Fig. 1a–c and Supplementary Information). We next investigated the functional relevance of the PAG1–SE interaction. Since the null mutation of *PAG1* (SALK_114864; *pag1-1*) has a defect in male gametogenesis⁶, we generated knockdown transgenic lines of *PAG1* by expressing artificial miRNA constructs. Approximately 82% (328 of 400) of

the 35S-amiR-PAGI transformants (hereafter referred to as pag1-2; Supplementary Information) exhibited developmental abnormalities with varying severities (Fig. 1c-g and Extended Data Fig. 2). The most severe lines (Type III, ~40% of transformants) had sword-shaped cotyledons and narrow, severely curled leaves. These seedlings displayed reddish petioles and leaves, suggestive of anthocyanin accumulation and accelerated plant ageing. Consistent with this speculation, these plants died soon after the emergence of a pair of true leaves. Lines with less severe

phenotypes (Type II, ~42% of transformants) also displayed narrow and strongly downward-curled cotyledons and rosette leaves, and flowers from these plants were twisted, with narrow sepals and petals separated by gaps; these plants were mostly sterile. Notably, these lines superficially phenocopied hypomorphic se and ago1 mutants29. Lines with mild developmental defects, which are represented by Type I, had slightly curled rosette leaves with frequent appearance of lobes or serration. These lines showed bush phenotypes with seemingly normal flowering times (Fig. 1d and Extended Data Fig. 2d). The sepals and petals turned around and appeared to lose adaxial and abaxial identity; however, their carpels and stamens remained fertile (Fig. 1e). The siliques from the mutant plants displayed an upside-down phenotype (Fig. 1f). The mutant pag1-2 also displayed severe defects in root growth, as cells from the root meristem and elongation regions were distorted and detached from each other (Fig. 1g and Extended Data Fig. 2e). Taken together, these data show that knockdown of PAG1 transcripts clearly impacted growth and development in Arabidopsis, with some defects generically observed in miRNA-pathway mutants.

Comparable impact of pag1 and se mutations on transcriptome profiling. We next examined whether PAG1 impacted SE-mediated RNA metabolism. RNA-seq analysis showed that the se mutation caused 5,602 differentially expressed genes (DEGs), whereas in pag1-2, the expression levels of approximately 5,000 genes were significantly either increased or decreased, respectively (Extended Data Fig. 3a). Such high numbers of DEGs in pag1-2 probably accounted for its pleotropic developmental defects. Gene Ontology (GO) analysis placed the DEGs of pag1-2 into numerous functional categories (Fig. 2a). The most impacted genes (3,907 of 9,985, 39.1%) are classified into metabolic processes that include generic metabolism (27.4%), proteasome assembly and catabolic processes (7.9%), and RNA metabolism (3.8%). These results imply that PAG1 is critical for maintaining the metabolic homeostasis of proteins and RNA, among other molecules. The second most impacted genes are involved in plant responses to stimuli (28.7%), suggesting that pag1-2 experiences intrinsic physiological disorders. The genes engaged in developmental processes (10.8%) are also highly impacted; this result is in line with the severe morphological abnormality of pag1-2. An additional significantly impacted group belongs to cellular trafficking and transport of proteins, including the cellular components that regulate nucleocytoplasmic transport (10.1%). These results suggest that loss of function of PAG1 might alter the cytoskeleton and the compositions or structures of membranes, including the nuclear envelope, as seen

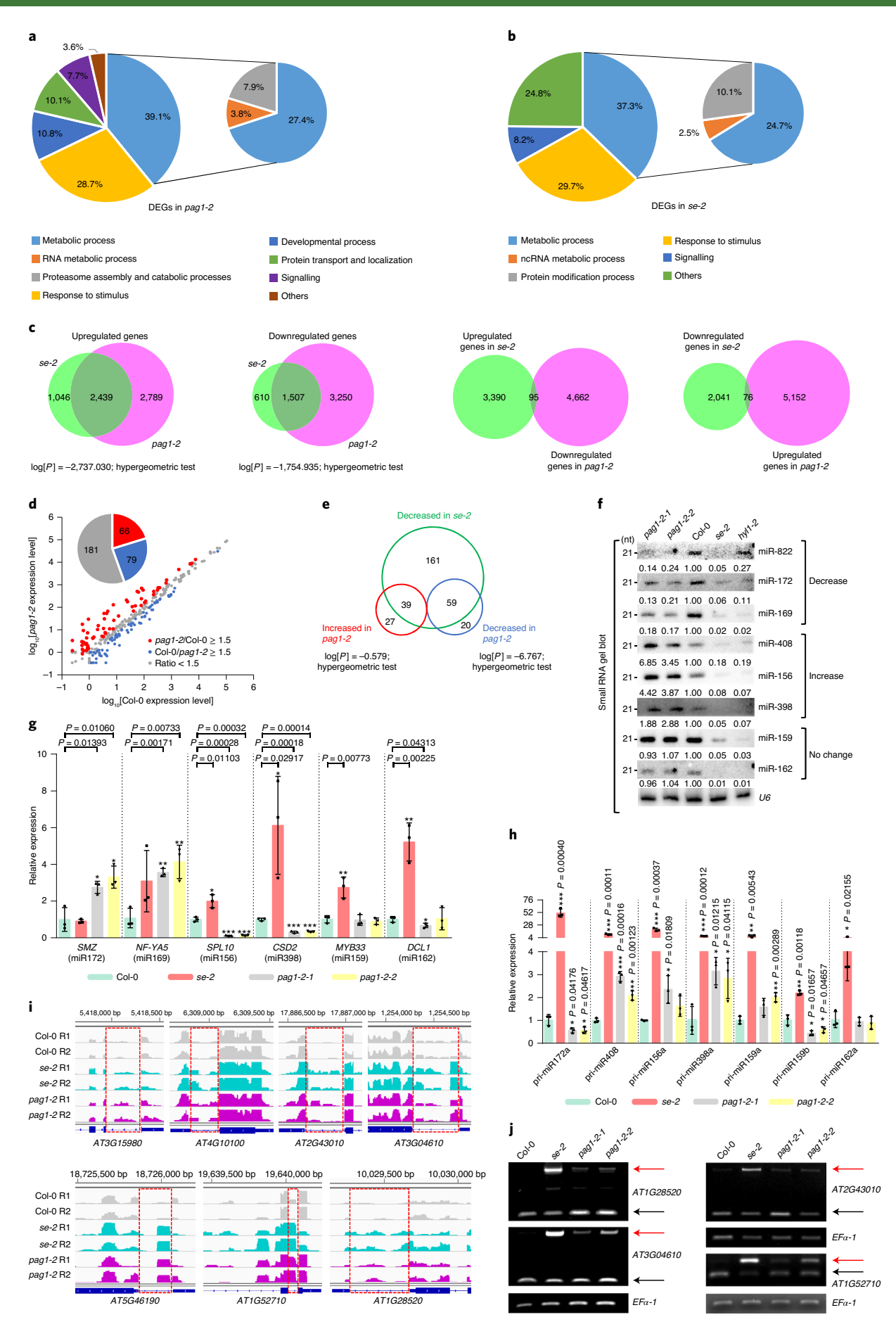
in root growth (Fig. 1g). Remarkably, GO analysis also revealed that SE-impacted genes are involved in metabolic processes as well, including RNA metabolism, protein modification and responses to stimuli (Fig. 2b).

Comparative analysis of the transcriptomes in se and pag1-2 revealed that among the 5,228 genes significantly upregulated in pag1-2, 2,439 (46.7%) were also upregulated in se-2. Conversely, among the 3,485 genes that were upregulated in se-2, 2,439 (70.0%) were also enhanced in pag1-2. The overlap of upregulated genes between pag1-2 and se-2 mutants is statistically significant $(\log(P) = -2.737.030;$ hypergeometric test) (Fig. 2c). Similarly, among the 4,757 downregulated genes in pag1-2, 1,507 (31.7%) were also repressed in the se-2 mutant. In parallel, among the 2,117 genes that were downregulated in se-2, 1,507 (71.2%) were also reduced in pag1-2. Downregulated genes also represent a significant overlap between pag1-2 and se-2 mutants (log(P) = -1,754.935; hypergeometric test) (Fig. 2c). The significantly overlapped DEGs displayed concomitant (or synchronized) patterns in se-2 and pag1-2, because only a few DEGs exhibited opposite expression patterns in se-2 and pag1-2 (Fig. 2c). Importantly, the significant overlapping of PAG1- and SE-impacted genes is meaningful rather than coincidental, as there was barely any overlapping of DEGs between se and apc8-1 (Extended Data Fig. 3d), a mutant that impacts thousands of transcripts and displays pleotropic phenotypes³⁰. Together, loss-of-function mutations of *PAG1* and *SE* had comparable impacts on transcriptome profiling, suggesting that PAG1 is genetically a positive regulator for SE.

Consistent but diversified impacts of *pag1* and *se* mutations on RNA processing. We next compared miRNA profiles in *se-2* and *pag1-2*. Whereas more than half of miRNAs remained relatively steady, 66 miRNAs exhibited at least a 1.5-fold increase and 79 exhibited at least a 1.5-fold reduction in *pag1-2* relative to Col-0 (Fig. 2d). Notably, both downregulated and upregulated miRNAs overlapped with the ones that depend on SE (Fig. 2e). The small RNA (sRNA)-seq results were readily validated by sRNA blot assays (Fig. 2f). Moreover, the targeted transcripts displayed opposite expression patterns to those of the deregulated miRNAs themselves (Fig. 2g).

To reconcile the diversified expression patterns of certain miR-NAs in *pag1-2* and *se-2*, we conducted a quantitative PCR with reverse transcription (qRT-PCR) analysis of expression for a few selected *MIR* genes. Interestingly, we found that the miRNAs that had constant or increased expression seemed to have stable or higher levels of pri-miRNAs, respectively (Fig. 2h). The synchronized accumulation of the tested pri-miRNAs and miRNAs in *pag1-2* suggested that *PAG1* mutation might have remarkable impacts on

Fig. 2 | PAG1 impacts SE-mediated RNA metabolism. a,b, GO enrichment analysis of the PAG1-regulated (a) and SE-regulated (b) DEGs. The numbers in or adjacent to the pies represent the ratios of genes in each category over the total DEGs. c, Overlapping of upregulated and downregulated genes between pag1-2 and se-2 mutants. See also Supplementary Tables 2 and 3. d, sRNA sequencing analysis of miRNA expression in Col-0 and pag1-2 mutants. The x and y axes indicate the logarithms of miRNA expression in Col-O and pag1-2, respectively. Compared with Col-O, miRNAs with at least 1.5-fold higher (pag1-2/Col-0 \geq 1.5) or lower (Col-0/pag1-2 \geq 1.5) expression in pag1-2 are indicated by red and blue dots, respectively. The grey dots indicate differences in expression level <1.5-fold (ratio <1.5). The pie in the top left of the chart indicates the numbers of different categories of miRNAs. See also Supplementary Table 4. e, Overlapping of up- and downregulated miRNAs in pag1-2 with SE-dependent miRNAs. In a-e, the data are derived from three biologically independent replicates. f, sRNA blot analyses of the selected miRNAs in the indicated mutants. U6 is a loading control. nt, nucleotides. The experiment was independently repeated twice with similar results. g, qRT-PCR analysis of selected miRNA targets in the indicated mutants. The data are presented as mean \pm s.d. n=3 biologically independent replicates. EF-1 α serves as an internal control. The asterisks indicate the significance of the differences between the mutants and the Col-0 control (*P < 0.05; **P < 0.01; ***P < 0.001; unpaired two-tailed Student's t-test). **h**, qRT-PCR analysis of pri-miRNAs. The data are presented as mean \pm s.d. n=3 biologically independent replicates. The asterisks indicate the significance of the difference between the mutants and the Col-O control (*P < 0.05; **P < 0.01; ***P < 0.001; unpaired two-tailed Student's t-test). i.j., Examples of the genes with the first intron retention defects. In i, the normalized expression of transcripts from the selected intron regions in Col-0, se-2 and pag1-2 is shown. The chromosome coordinates (top) and gene names (bottom) are shown on each panel. The rectangles mark introns with higher retention in se-2 and pag1-2. Two biological replicates for each sample are shown. bp, base pairs. In j, RT-PCR validation of alternative splicing of selected genes in Col-O and the indicated mutants is shown. EF- 1α serves as an internal control. The red and black arrows indicate the unspliced and spliced forms, respectively. The experiment was independently repeated twice with similar results.



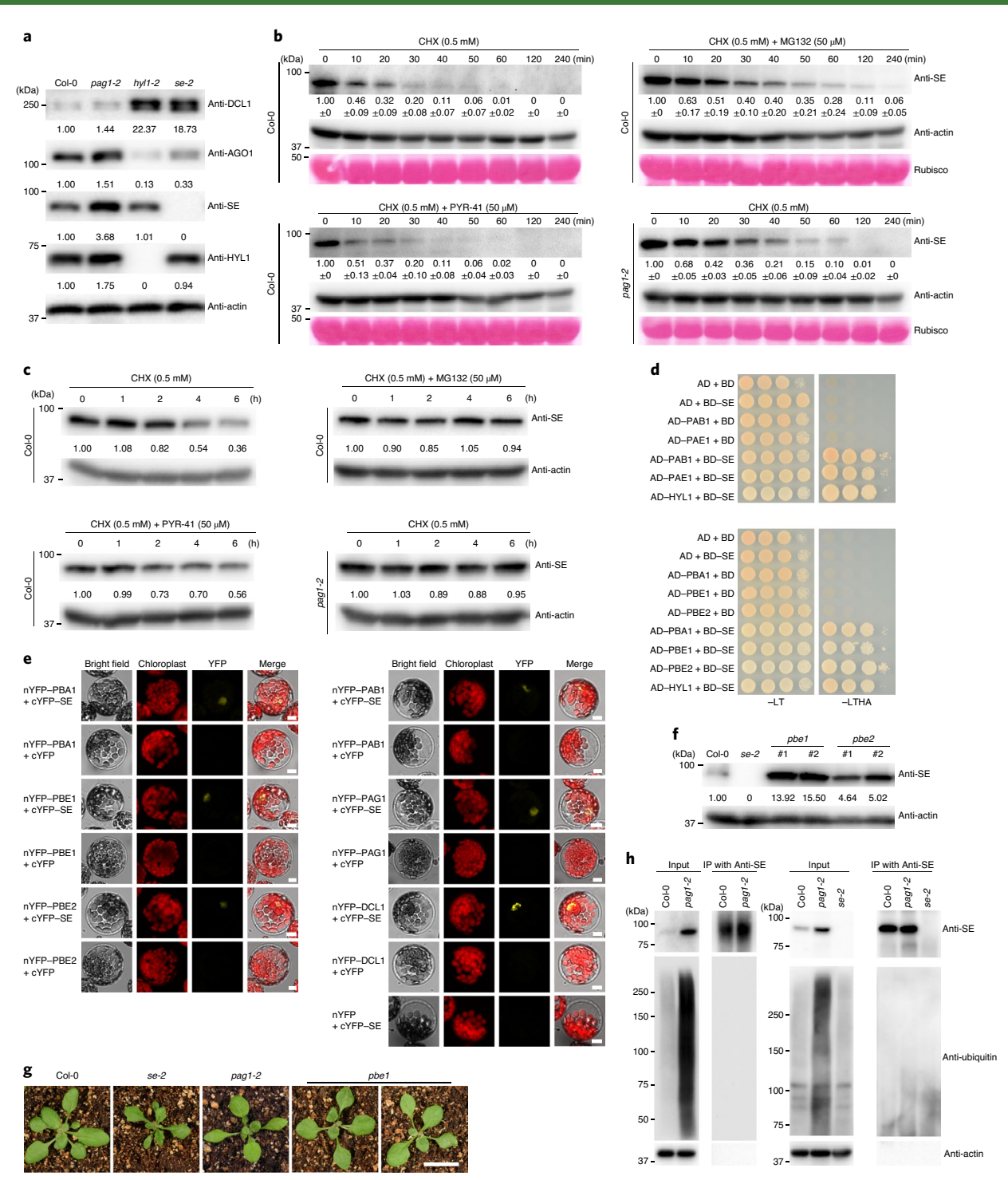


Fig. 3 | SE is degraded via PAG1-containing 20S proteasome, but not through the ubiquitin-proteasome pathway. a, Western blot analysis of key components of the miRNA pathway in pag1-2 using antibodies specifically against the indicated proteins. Actin is a loading control. b, In vitro cell-free SE-decay assay. Total proteins from Col-0 and pag1-2 were extracted and incubated with CHX (0.5 mM) with or without 50 μM MG132 or 50 μM PYR-41 for the indicated times. SE levels were determined with an anti-SE antibody. Actin and Rubisco serve as loading controls. c, In vivo SE-decay assay. Col-0 and pag1-2 seedlings were treated with CHX (0.5 mM) with or without 50 μM MG132 or 50 μM PYR-41 for the indicated times. SE levels were determined with an anti-SE antibody. Actin is a loading control. d,e, Y2H (d) and BiFC (e) assays showed interactions between SE and additional 20S proteasome subunits, including PAB1, PAE1, PBA1, PBE1 and PBE2. See also Extended Data Fig. 6 for negative controls. In e, a combination of 35S-cYFP-SE and 35S-nYFP-DCL1 serves as a positive control. Scale bars, 10 μm. At least ten independent colonies (d) and protoplasts (e) were tested for each interaction combination and showed similar results. f, Western blot analysis of SE protein levels in pbe1 and pbe2 mutants using an anti-SE antibody. Actin serves as a loading control. g, Leaf morphological phenotypes of 21-d-old Col-0, se-2, pag1-2 and pbe1. Scale bar, 1cm. h, Western blot analysis shows that ubiquitin is not attached to immunoprecipitated SE protein from Col-0, se-2 and pag1-2. Ubiquitin was detected with two different anti-ubiquitin antibodies (purchased from Santa Cruz Biotechnology (left) and Agrisera (right)). In a-c, the numbers below the images indicate the relative mean signals of SE protein at different time points that were sequentially normalized to those of SE and actin at time 0, where the value was arbitrarily assigned a value of 1 with or without ± s.d. The experiments were independently repeated twice (c,f,g) or three time

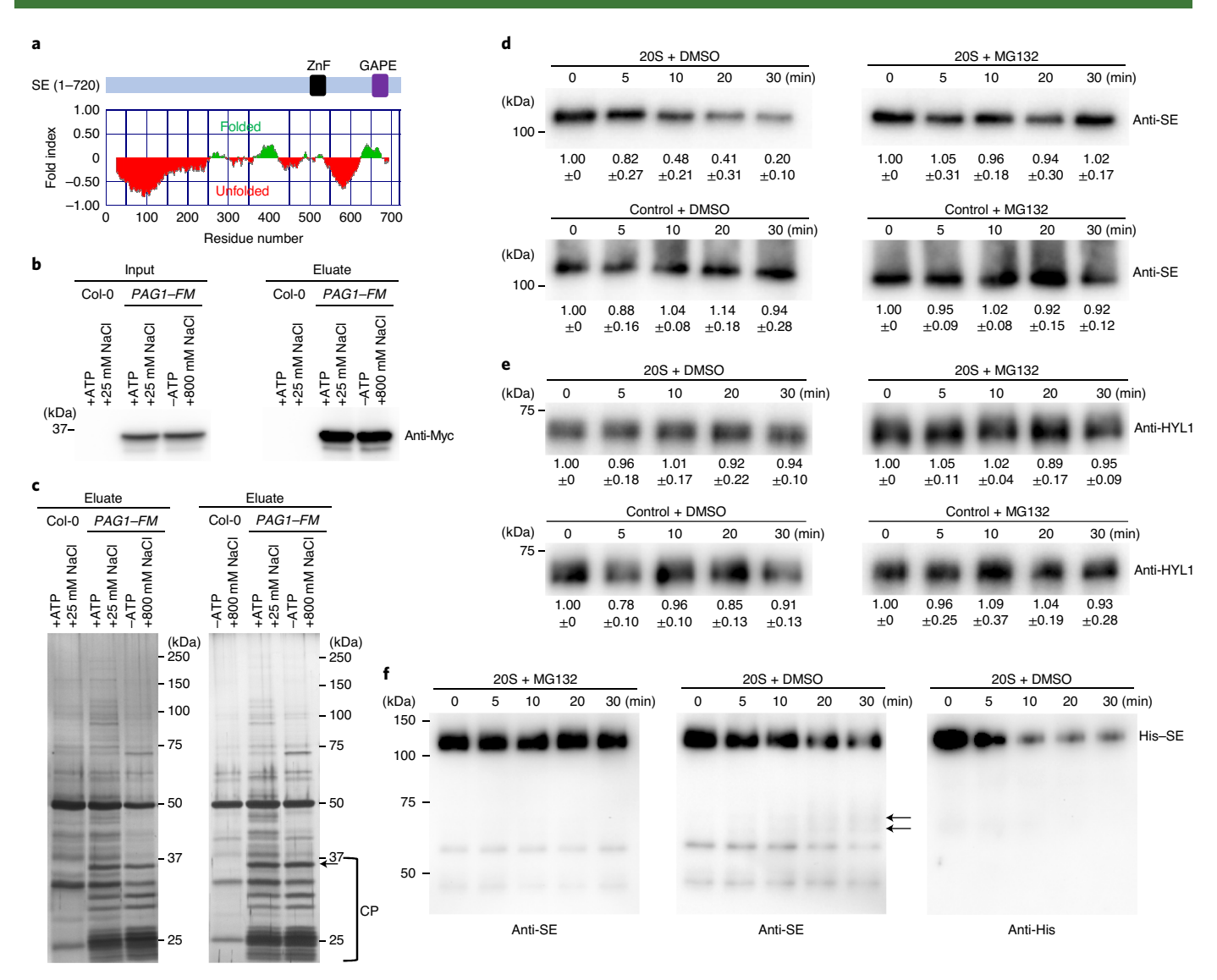


Fig. 4 | In vitro degradation of SE by purified *Arabidopsis* **20S proteasome. a**, Computational analysis through the FoldIndex algorithm predicts that SE is an IDP. Regions with green or red colouring indicate the folded or unfolded domains, respectively. **b**, Western blot analysis of affinity-purified PAG1 complexes from *Arabidopsis*. Total protein extracts from 10-d-old Col-0 and P_{PAG1} -FM plants were incubated with anti-FLAG M2 affinity beads, in the presence or absence of ATP, with 25 mM or 800 mM NaCl. PAG1-FM complex was eluted with the FLAG peptide. Immunoprecipitated PAG1-FM was detected with western blot analysis using an anti-Myc antibody. **c**, Two silver-staining examples of immunoprecipitated PAG1-FM-containing 20S and 26S proteasomes resolved in SDS-PAGE (left and right panels). IP was conducted in the conditions indicated above the gels. The arrow and bracket indicate PAG1-FM proteins and subunits of the 20S core proteasome (CP), respectively. **d,e**, In vitro reconstitution assays of protein degradation via 20S proteasome. Recombinant 6xHis-SUMO-SE and HYL1 proteins were incubated with the PAG1-FM immunoprecipitate or control IP prepared from P_{PAG1} -FM transgenic plants or Col-0, respectively. The reaction mixture was applied with either dimethylsulfoxide (DMSO) or 50 μ M MG132 and stopped at the indicated time intervals. HYL1 serves as a negative control. The numbers below the gels indicate the relative mean signals of SE or HYL1 proteins at different time points that were normalized to those of the proteins at time 0, where the value was arbitrarily assigned a value of 1 with \pm s.d. from three experiments. **f**, Detection of truncated forms of 6xHis-SUMO-SE protein by 20S proteasome in vitro by anti-His or anti-SE antibodies. The arrows indicate degraded SE. Note that the anti-SE antibody is raised against a peptide located in the zinc-finger domain. The experiments were independently repeated three times (**b,c,f**) with similar results.

the transcription of certain miRNA loci, and such impacts might mask its effect on downstream SE-mediated miRNA biogenesis.

We further assessed whether PAG1 impacted SE-mediated pre-mRNA splicing. We pinpointed numerous splicing defective transcripts in *se-2* according to IGV files. Importantly, these abnormal splicing events were also detected in RNA-seq and RT-PCR assays of *pag1-2* (Fig. 2i,j). The results indicated that PAG1 indeed impacted SE-mediated pre-mRNA splicing.

SE also acts as a transcriptional factor for numerous protein-coding genes and transposable elements. We mined our previous SE-ChIP-seq data from a seedling stage²⁵ and compared SE

binding loci and *PAG1*-regulated genes. This comparative analysis showed that among 9,985 of *PAG1*-regulated genes, 2,250 overlapped with SE-binding loci, representing 36.5% of SE-regulated transcriptional events ($\log(P) = -8.167$; hypergeometric test) (Extended Data Fig. 3e). It is thus reasonable to speculate that a substantial portion of *PAG1*-deregulated genes might be regulated via the impact of *SE*-controlled transcriptional regulation.

PAG1 targets SE for degradation, but not through a ubiquitin-proteasome pathway. PAG1 is a component of 26S proteasome and might regulate SE accumulation. Indeed, western blot

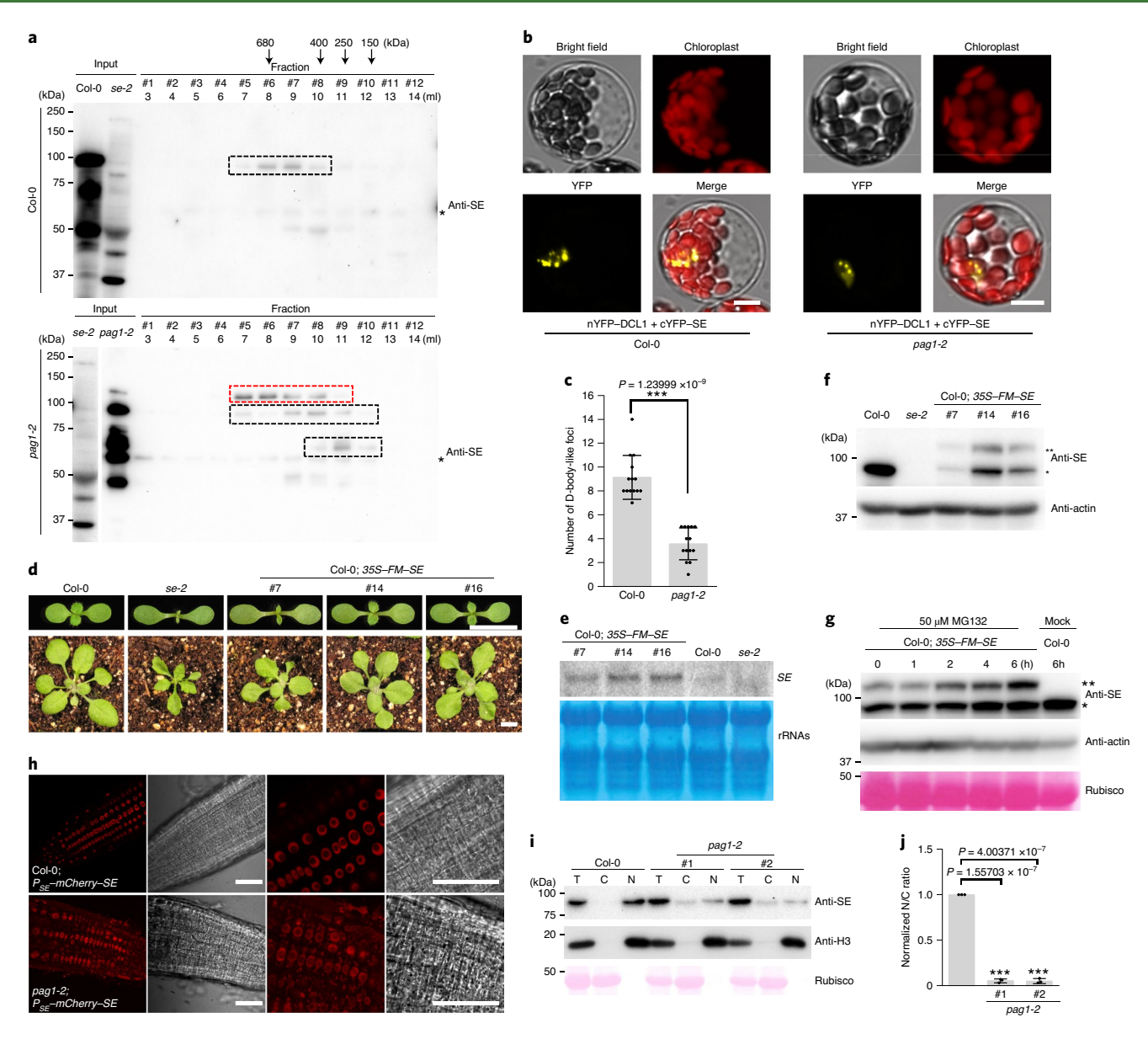


Fig. 5 | Overaccumulation of disordered SE protein interferes with its normal function. a, SEC shows different forms of SE protein in Col-0 and pag1-2 plants. Total protein extracts were resolved through a Superdex 200 10/300 GL column, and eluates were detected via western blot analysis using an anti-SE antibody. Eluate fractions, volumes and molecular weight standards are shown on top of the panel. The bands framed in the black dashed boxes are full-length or truncated SE proteins. The bands framed in the red dashed box are an unknown modified form of SE protein. Asterisks indicate unspecific bands. **b**, BiFC assays showed that the assembly of SE/DCL1-contained microprocessors is compromised in pag1-2 compared with Col-0. 35S-nYFP-DCL1 and 35S-cYFP-SE constructs were transfected into protoplasts prepared from Col-O and pag1-2, and the YFP signal indicated the interaction of DCL1 and SE. Scale bars, 10 µm. At least 14 independent protoplasts for each interaction were examined and showed similar results. c, Statistical analysis of numbers of D-body-like foci in Col-0 and pag1-2. The data are presented as mean \pm s.d.; n = 14 biologically independent samples. The asterisks indicate the significance of the differences between pag1-2 and Col-0 (***P<0.001; unpaired two-tailed Student's t-test). **d**, SE overexpression transgenic lines phenocopied se mutants; 10-d-old (top) and 21-d-old (bottom) Col-0; 35S-FM-SE transgenic plants are shown. Note that the phenotypes of Col-0; 35S-FM-SE had various degrees of recovery at adult stages. Scale bars, 0.5 cm. e, RNA blot analysis shows that SE transcript is accumulated in Col-0; 35S-FM-SE transgenic plants. Ribosomal RNAs are the loading control. f, Western blot analysis using an anti-SE antibody shows that both endogenous and transgenic SE proteins were reduced in Col-0; 35S-FM-SE transgenic plants. Actin is the loading control. Single and double asterisks indicate endogenous SE and FM-SE, respectively. g, Western blot analysis shows that transgenic SE triggered concurrent degradation of both endogenous and transgenic SE proteins via proteasome. Col-0; 35S-FM-SE transgenic plants were treated with MG132 at the indicated times, and SE protein was detected using an anti-SE antibody. Actin and Rubisco were used as loading controls. h, Confocal imaging assays show the different localizations of SE in the nucleus and cytoplasm in Col-O and pag1-2 backgrounds. Scale bars, 50 μm. i, Cell-fractionation analysis shows SE amount in total extraction (T), nuclear fraction (N) and cytoplasmic fraction (C) from Col-O and pag1-2 plants. Western blot analysis was conducted with an anti-SE antibody. Rubisco stained with Ponceau S and histone 3 detected by anti-H3 antibody were used as controls for the cytoplasmic- and nuclear-specific fractions, respectively. j, Quantification of the nuclear-cytoplasmic distribution of SE protein. The nuclear and cytoplasmic fraction ratios (N/C) of SE protein in pag1-2 were sequentially normalized to that of Col-0, which was arbitrarily assigned a value of 1. The data are presented as mean \pm s.d.; n=3 biologically independent replicates. The asterisks indicate the significance of the differences between the mutant and Col-0 (***P < 0.001; unpaired two-tailed Student's t-test). The experiments were independently repeated twice (e,g) or three times (a,d,f,h) with similar results.

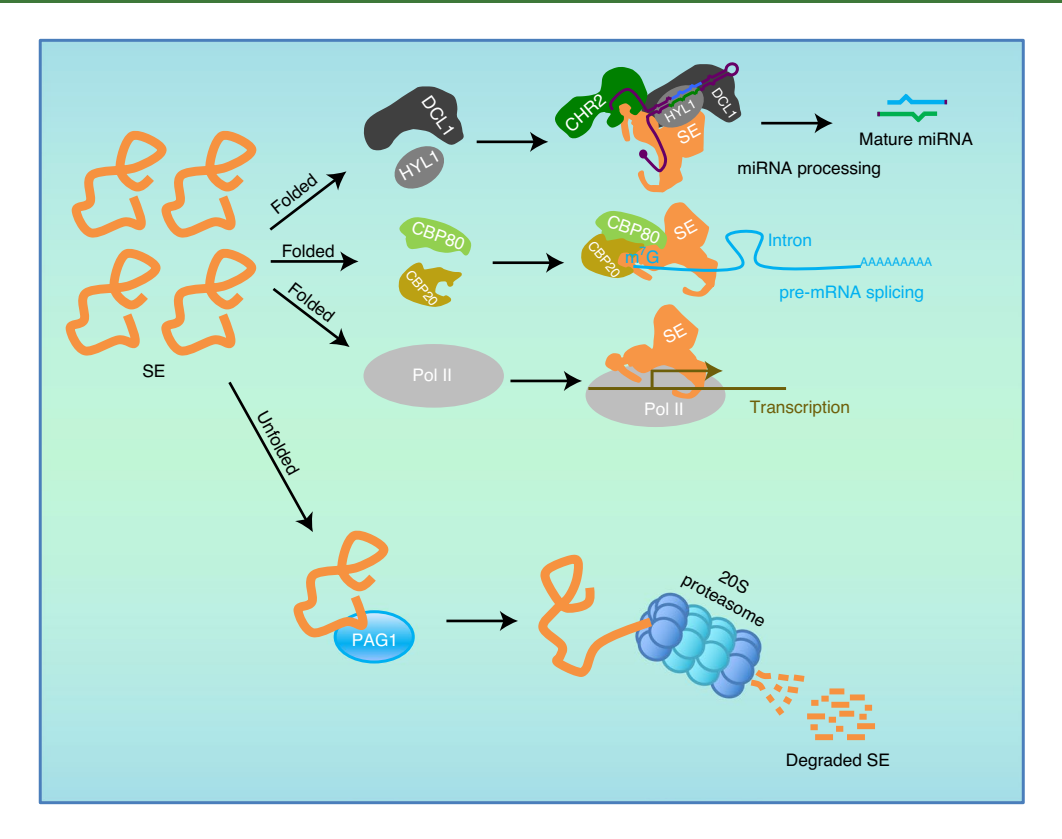


Fig. 6 | Proposed model for the degradation of SE protein by PAG1. This model shows that PAG1 acts as a surveillance mechanism to destroy excess unstructured SE protein via the 20S proteasome pathway to secure the functionality of folded SE, which is assembled and protected in macromolecular complexes.

assays showed that SE protein was clearly increased in *pag1-2* relative to Col-0 (Fig. 3a). Moreover, SE accumulation was positively correlated with the phenotypic severity of the mutants (Extended Data Fig. 4a). Other components in the miRNA pathway such as AGO1 and HYL1 also marginally accumulated in the mutants (Fig. 3a). This observation suggests that one component mutation might affect the expression of other components in the miRNA pathway³¹.

We further investigated the protein stability of SE by adopting a method for in vitro protein decay³². We prepared cell lysates from ten-day-old Col-0 seedlings and treated the extracts with cycloheximide (CHX) to block protein synthesis. SE protein had a half-life of approximately 10 min in the absence of new protein synthesis, indicating that SE is indeed a very unstable protein (Fig. 3b and Extended Data Fig. 4b,c). However, the addition of MG132 (a potent proteasome inhibitor) to the reaction mixture substantially inhibited the degradation of SE and extended the half-life of SE to approximately 20 min (Fig. 3b and Extended Data Fig. 4b,c). These results suggest that the SE protein is destroyed in vivo by proteasomes. Notably, MG132 did not completely block the degradation, implying that SE could also be degraded by an unidentified cellular protease. When we conducted the assay with the extracts from pag1-2, we found that the half-life of SE protein was also substantially extended (Fig. 3b and Extended Data Fig. 4b,c). This result indicated that proteasome-mediated SE degradation involves PAG1 in Arabidopsis.

Protein degradation can be fulfilled through ubiquitin-dependent 26S proteasome and/or ubiquitin-independent 20S core proteasome. To study which proteasome accounts for SE degradation, we cotreated the cellular extracts with CHX and PYR-41, a protease inhibitor of ubiquitin-activating enzyme E1 that can selectively impede the activity of 26S proteasome, but not 20S proteasome. In this scenario, SE was again destroyed quickly, as observed in the scenario without any protease inhibitor (Fig. 3b and Extended

Data Fig. 4b,c). This result suggests that SE degradation might be through the PAG1-containing 20S proteasome. We then treated ten-day-old seedlings with CHX and with or without proteasome inhibitors (MG132 or PYR-41) and then measured SE levels in vivo. Again, SE was readily destroyed in the absence of protein synthesis in Col-0. However, this degradation was inhibited or delayed either by MG132 treatment or in *pag1-2* (Fig. 3c and Extended Data Fig. 4d). Moreover, the inhibitory process of SE degradation was not deterred by PYR-41 (Fig. 3c and Extended Data Fig. 4d). This result was in contrast to that of DMS3 protein³⁰, a positive control that is degraded by the 26S proteasome (Extended Data Fig. 5a). Altogether, these results support the notion that SE degradation occurs through the PAG1-containing 20S proteasome.

One prediction from the model of SE degradation via 20S proteasome is that SE will interact with additional 20S proteasome subunits. To test this, we randomly cloned a few components of 20S proteasome and conducted yeast-two-hybrid (Y2H) and bimolecular fluorescence complementation (BiFC) assays. The two assays showed that SE indeed interacted with PAB1, PAE1, PBA1, PBE1 and PBE2, but not PAC1, PAF1, PBD1 or the 19S regulatory subunit RPN1a (Fig. 3d,e and Extended Data Fig. 6), indicating that SE binds to 20S proteasome complex. We then obtained two mutants of 20S proteasome (pbe1 and pbe2) and observed that SE was dramatically accumulated in pbe1 and moderately increased in pbe2 in the adult stages (Fig. 3f). In lines with the SE accumulation, pbe1 phenocopied the weak alleles of pag1-2 in certain aspects such as rhomboid cotyledons and slow-growing and curved leaves (Fig. 3g). The mutant pbe2 lacks obvious developmental defects, probably because PBE1 and PBE2 are functionally redundant but PBE1 expression is tenfold higher than that of PBE2 in planta³³. All together, we concluded that SE is degraded through 20S proteasome in vivo.

Finally, we probed the SE immunoprecipitates with anti-ubiquitin antibodies from different resources. Although we

detected overwhelmingly accumulated ubiquitin-conjugated cellular proteins in the input fractions, we were unable to detect ubiquitin-attached SE protein (Fig. 3h). This was probably not due to potential technical pitfalls, as we could easily detect the positive control, a ubiquitin-binding DMS3 protein, in parallel experiments (Extended Data Fig. 5b). These results thus further validated the idea that SE is degraded through a ubiquitin-independent 20S proteasome pathway in vivo.

20S proteasome degrades SE in vitro. Computational modelling via FoldIndex analysis³⁴ revealed that SE protein contains two or three major patches of intrinsically unfolded regions that cover 254 and 137 amino acid residues at the N- and C-terminal parts, respectively (Fig. 4a and Extended Data Fig. 7a). This prediction is consistent with a structural analysis that only a core domain (194–543 amino acids) containing a zinc-finger motif of SE protein can be crystallized¹⁴. SE is thus an IDP and can be targeted by 20S proteasome.

To further study the biochemical mechanism of SE degradation, we adopted an in vitro 20S proteasome reconstitution system following the previously published protocol^{6,35}. Briefly, we immunoprecipitated PAG1 complexes from total protein extracts of stable transgenic lines expressing PAG1-Flag-4Myc (PAG1-FM) under its native promoter in two different conditions. In one condition, the protein extract was applied with ATP in a lower-salt condition, aiming for the isolation of 26S proteasome because the integrity of the complex relies on ATP. By contrast, the other protein extracts were not applied with ATP, and immunoprecipitates (IPs) were washed with a buffer containing 800 mM NaCl, aiming for the isolation of 20S proteasome alone, as this stringent condition would strip the 19 regulatory subunits away from the core 20S proteasome. The western blot and silver stain assays showed that both Arabidopsis 20S and 26S proteasomes were purified successfully, and the patterns of proteasome subunits were similar to those described previously (Fig. 4b,c). We next used the substrate succinyl-Leu-Leu-Val-Tyr-7-amido-4-methylcoumarin (Suc-LLVY-AMC) as a positive control to detect the proteasome activity and found that purified 20S proteasome, but not a control IP, showed strong activity (Extended Data Fig. 7b). This result indicated that the reconstitution system of 20S proteasome worked efficiently. In this scenario, we applied recombinant SE protein (Extended Data Fig. 7c) with the isolated 20S proteasome. A western blot analysis showed that SE was indeed readily degraded by PAG1-containing 20S proteasome but not by the control IP using Col-0 plants (Fig. 4d and Extended Data Fig. 7e). Moreover, truncated forms of SE protein were detected through a time course when an anti-SE antibody that targets the zinc finger domain (amino acids 498 to 523) was used, but not with an anti-His antibody that targets the N-terminal 6xHis epitope. This result suggests that 20S proteasome primes SE degradation, probably though its N-terminal disordered part, while binding the C-terminal part of SE (Figs. 1b and 4a,f and Extended Data Fig. 7g). Importantly, the SE degradation was largely attenuated by MG132. These results were clearly not technical artefacts because a control protein, HYL1 (Extended Data Fig. 7d), which is well folded, was unlikely to be destroyed by the isolated 20S proteasome in vitro (Fig. 4e and Extended Data Fig. 7f). We therefore concluded that PAG1-containing 20S proteasome is responsible for SE turnover in vitro.

Excess amount of SE protein interferes with its native function. Whereas PAG1 biochemically targets SE for degradation in vivo and in vitro (Figs. 3b,c and 4d), *PAG1* is genetically a positive regulator for SE (Fig. 2). This inconsistency prompted us to examine the dif-

in vitro (Figs. 3b,c and 4d), *PAG1* is genetically a positive regulator for *SE* (Fig. 2). This inconsistency prompted us to examine the differences in SE profiling between *pag1-2* and Col-0. Size-exclusion chromatography (SEC) showed that recombinant His-SUMO-SE

protein was eluted approximately at a molecular mass of 189kDa, suggesting a formation of SE dimerization in vitro (Extended Data Fig. 7c). In contrast, the major peak of SE protein from Col-0 extracts was located in fractions 6 and 7, which corresponded to a molecular mass of approximately 680 kDa (ref. 17) (Fig. 5a). This SEC distribution indicated that SE forms macromolecular complexes with other cellular proteins and/or nucleic acids, and SE in complexes is thus considered properly folded and functional (Fig. 5a). In pag1-2, by contrast, SE was distributed in a broader range from macromolecular complexes to low-molecular-weight regions, which represented unpacked SE protein. Furthermore, a large portion of SE protein was in truncated forms in the low-molecular-weight portions with sizes similar to the ones observed in in vitro assays (Figs. 4f and 5a and Extended Data Fig. 7g). These results indicate that the protein is degraded through 20S proteasome when unpacked. We have repeatedly detected isoforms of SE protein in pag1-2 (Fig. 5a, red dashed box). We have excluded the possibility of post-translational modifications such as ubiquitination (Fig. 3h). Further research is needed to determine whether the isoform of SE represents a marker for 20S proteasome targeting or a new role of 20S proteasome (such as an emerging transpeptidation event)7.

The SEC results also suggested that there are different pools of SE protein in planta: some portion of SE is improperly folded and unprotected, whereas the others are assembled and functional; and the overaccumulated, unstructured SE protein might compete with cellular partners and interfere with the functional SE protein that is in macromolecular complexes. To test this, we cotransfected nYFP-DCL1 and cYFP-SE into protoplasts of Col-0 and pag1-2 and examined SE-DCL1 interaction patterns. The complementation of cYFP-SE and nYFP-DCL1 formed numerous foci in the nucleus, reminiscent of previously reported D-bodies in Col-0 (ref. 36). However, the number of D-body-like foci was substantially reduced in pag1-2 (Fig. 5b,c and Extended Data Fig. 8). This result indicated that accumulated SE protein did impact the formation of microprocessors, contributing to abnormal miRNA production (Fig. 2d-f). This result also underscored the comparable molecular and developmental defects between se and pag1-2 (Figs. 1 and 2).

We further revisited the transgenic plants overexpressing FM-SE (Col-0; 35S-FM-SE). The FM tag should not affect SE function, as FM-SE controlled by a native promoter fully rescued the se mutant²⁵. Intriguingly, 95% of Col-0; 35S-FM-SE transgenic lines exhibited developmental defects similar to loss-of-function se and pag1 mutants, especially in the early seedling stage (Fig. 5d). The comparable phenotypes of SE overexpression lines and se mutants did not simply result from the cosuppression in the transgenic plants, because transgenic SE was in a full-length form and also significantly accumulated compared with the amount of endogenous SE (Fig. 5e and Extended Data Fig. 9a). Rather, we observed that both endogenous and transgenic SE protein were substantially reduced (Fig. 5f). Moreover, MG132 treatment could largely restore the accumulation of transgenic and endogenous proteins (Fig. 5g). This result indicates that excess transgenic SE protein alters the pool balance of unstructured and folded SE protein in vivo and interferes with the assembly of functional SE-engaged complexes, and that such disturbance triggers the degradation of both endogenous and transgenic SE protein and leads to defects in molecular and morphological phenotypes of Col-0; 35S-FM-SE. This scenario is reminiscent of the observations in *pag1-2*.

PAG1 mutation causes mislocation of SE. Since *PAG1* mutation causes the reprogramming of numerous protein trafficking genes, one possibility is that the cellular compartmentalization of SE might be altered. To test this, we revisited the cellular distribution of SE protein in Col-0 and pag1-2 using confocal assays. Native SE protein was predominantly distributed in the nucleus in the stable transgenic plants expressing Col-0; P_{SE} -mCherry-SE. However, SE could

be easily detected in both the nucleus and cytoplasm in *pag1-2* (Fig. 5h). This observation could be validated by a nuclear–cytoplasmic fractionation assay³¹ (Fig. 5i,j and Extended Data Fig. 10). The results thus suggest that SE protein might be stacked into the cytoplasm in *pag1-2* because the cells are deformed, and the nucleus–cytoplasm borders might be ruined in the mutant.

Discussion

Here we reported that PAG1 directly recruits SE protein to 20S core proteasome for degradation via a ubiquitin-independent mechanism in *Arabidopsis*. Several lines of evidence support our model: (1) SE physically binds PAG1 and additional components of 20S proteasome (Figs. 1a,b and 3d,e and Extended Data Fig. 1a-c); (2) SE accumulates in the mutants of 20S proteasome subunits (Fig. 3a,f and Extended Data Fig. 4a), and this accumulation is due to the extended half-life of SE in the mutants (Fig. 3b,c and Extended Data Fig. 4b-d); (3) the broad proteinase inhibitor MG132, but not the 26S proteasome inhibitor PYR-41, delays the half-life of SE (Fig. 3b,c and Extended Data Fig. 4b-d); (4) the conjugation of ubiquitin to SE protein is not detectable even in pag1-2 (Fig. 3h); and (5) the 20S core proteasome isolated from in vivo can readily destroy SE protein without ATP (Fig. 4d,f and Extended Data Fig. 7e,g). Intriguingly, PSMA3 (α7 subunit), the mammalian orthologue of PAG1, is also associated with Ars2 (ref. ³⁷), suggesting that the orthologue of SE might be similarly destroyed through PSMA3-contained 20S proteasome in animals, with a further suggestion that PAG1/PSMA3-mediated SE/Ars2 degradation through 20S proteasome complex might be evolutionally conserved through the eukaryotes.

SE protein undergoes ubiquitin-independent degradation due to its inherent feature as an IDP. IDPs are prone to destruction independent of the ubiquitin-mediated 26S proteasome pathway; such scenarios have been documented in several mammalian and yeast proteins^{38–41}, but not in plants. In SE protein, whereas the middle part of the protein can be folded, a large portion of the N-terminal region is disordered and unstructured14 and thus could act as a degradation signal (Fig. 4a). Although SE is susceptible to 20S proteasomal degradation, we have no reason to exclude the possibility that other factors of 26S proteasome, especially the 19S regulatory subunits, play any role in SE turnover. As the middle domain of SE is folded into a walking man-like structure¹⁴, some of the 19S regulatory subunits might contribute to the unfolding of the folded part of SE protein and further facilitate its degradation. In fact, the cooperativity of both 20S and 26S proteasomes has been observed in the degradation of some mammalian proteins via the ubiquitin-dependent and ubiquitin-independent mechanisms8.

Whereas PAG1 mechanistically degrades SE, it genetically promotes SE function. This superficial paradox implies that what PAG1 clears is disordered and non-functional SE in vivo, rather than folded and functional SE, which is typically assembled into macromolecular complexes (Fig. 6). This notion is supported by the fact that the truncated forms of SE are associated only with the fractions of low molecular mass, whereas SE is intact in the fractions of the macromolecular complexes in the SEC assays (Fig. 5a). In fact, a prevailing view is that IDPs, when isolated, are disordered and subject to degradation via 20S proteasome. However, the proteins are protected from 20S proteasomal degradation in vivo via a process of folding-on-binding (or masking of their unstructured regions) on interaction with other cellular factors⁴². It has been speculated that the interactions between IDPs and their partners are specific but often have low affinities. These properties give IDPs the flexibility to bind different partners, or quickly switch between partners when needed, to tackle various tasks9. Thus, IDPs should be in dynamic equilibrium between free form and structured status. This notion can be highlighted by the fact that SE degradation is mostly inhibited by MG132 but not by PYR-41 under normal physiological conditions (Fig. 3c). One could also imagine that the disturbance of the equilibrium between unfolded and folded forms of IDPs would damage the integrity of the IDP complexes, leading to their malfunctions^{7,8}. The proper maintenance of this equilibrium is extremely important for the IDPs that form parts of numerous complexes, and any excess or shortage of one of the subunits might impact the assembly of the macromolecular complexes and interfere with their biological functions^{7,8}. This scenario applies to the multifunctional SE protein and is highlighted by the fact that overaccumulated SE protein in pag1-2 and overexpression of SE in the 35S–FM–SE transgenic lines display comparable molecular and/or morphological defects relative to se. We could thus envisage that the excess unstructured SE behaves as a dominant-negative form, disrupts the homeostatic balance and interferes with functional SE complexes. Under these circumstances, the prompt clearance of the free form through 20S proteasome represents an elegant mechanism to secure SE-scaffolded macromolecular complexes so that they can fulfill their multiple functions.

Methods

Plant materials and growth conditions. The *Arabidopsis thaliana* ecotypes Columbia (Col-0), *se-2* (SAIL_44_G12), *hyl1-2* (SALK_064863), *dcl1-9* (CS3828), *pbe1* (SALK_092686) and *pbe2* (SALK_004669) used in this study were described previously^{17,33}. Binary vectors including pBA002a–P_{PAGI}–gPAG1–eYFP, pBA002a–P_{PAGI}–gPAG1–FM and pBA–35S–amiR–PAG1 were transformed into the Col-0 ecotype of *A. thaliana* by the floral-dip transformation method⁴³. The T2 transgenic lines containing the tagged PAG1 were screened by western blot analysis or confocal microscopy. Transgenic plants of *pBA–35S–amiR–PAG1* (*pag1-2*) were screened for the presence of artificial miRNAs and the decrease of target transcripts in T1 transgenic plants using an sRNA blot or qRT–PCR assay, respectively. Wild-type (Col-0), mutant and transgenic lines were grown under a 12h light, 12h dark cycle as previously described⁴⁴.

Construction of vectors. Most of the plant binary constructs in this paper were made using a Gateway system (Invitrogen). The destination vectors pBA-DC-YFP, pBA-DC, pBA002a-DC-YFP and pBA002a-DC-Flag-4Myc were used for transient expression in *N. benthamiana* or the stable transformation of *A. thaliana* as described previously⁴⁵. Complementary DNA, DNA and artificial miRNA genes were cloned into pENTR/D-TOPO vectors (Invitrogen) using the primers listed in Supplementary Table 1, and were confirmed by sequencing before being transferred to the appropriate destination vectors by recombination using LR Clonase (Invitrogen).

pBA-PAG1-YFP was constructed as follows: *PAG1* coding sequences were amplified using a KOD polymerase from *Arabidopsis* (Col-0) cDNAs and then cloned into pENTR/D-TOPO vectors to obtain pENTR/D-PAG1. Finally, pENTR/D-PAG1 vector was transferred into pBA-DC-YFP by the LR reaction to yield pBA-PAG1-YFP.

pBA002a- P_{PAGI} -gPAG1-YFP and pBA002a- P_{PAGI} -gPAG1-FM were constructed as follows: native promoters of PAG1 and PAG1 genomic fragments were amplified using a KOD polymerase with Col-0 genomic DNA as a template and the primers listed in Supplementary Table 1. They were then cloned into pCR-BluntII-TOPO vectors (Invitrogen) to generate pBlunt- P_{PAGI} -gPAG1 vector. Next, NotI/AscI-digested P_{PAGI} -gPAG1 fragments were ligated into NotI/AscI-digested pENTR/D to yield pENTR/D- P_{PAGI} -gPAG1. Then, P_{PAGI} -gPAG1 was transferred into pBA002a-DC-eYFP and pBA002a-DC-Flag-4Myc by the LR reaction to create pBA002a- P_{PAGI} -gPAG1-eYFP and pBA002a- P_{PAGI} -gPAG1-FM, respectively.

Y2H assays. All of the tested cDNAs were cloned into the Gateway compatible vectors pGADT7–DC and pGBKT7–DC by the LR reaction. Different combinations of constructions were then transformed into the yeast strain AH109. The Y2H assays were performed as previously described¹⁷.

BiFC assays. The isolation and transfection of *Arabidopsis* leaf protoplasts from four-week-old Col-0 and *pag1-2* plants were performed as described previously¹⁶. cYFP–SE (SE fused with C-terminal YFP) was coexpressed with nYFP–PAB1, nYFP–PBB1, nYFP–PBE1 and nYFP–PBE2 (PAB1, PAG1, PBA1, PBE1 and PBE2 fused with N-terminal YFP) in the protoplasts. Twelve hours after transfection, the fluorescence signals in the protoplasts were visualized using Leica SP8 confocal microscopy. YFP and chlorophyll fluorescence signals were excited at 514 and 633 nm, respectively. Combinations of nYFP+cYFP–SE, cYFP+nYFP–PAB1, cYFP+nYFP–PAG1, cYFP+nYFP–PBA1, cYFP+nYFP–PBE1 and cYFP+nYFP–PBE2 were used as negative controls. A combination of nYFP–DCL1+cYFP–SE was used as a positive control.

Luciferase complementation imaging assays. All of the tested cDNAs were cloned into pCAMBIA-nLuc and pCAMBIA-cLuc by the LR reaction. All of the constructs were then transformed into *Agrobacterium tumefaciens* strain ABI. The luciferase complementation imaging assays were performed as previously described³¹.

Fluorescence resonance energy transfer assays and confocal microscopy.

Agrobacterium harbouring pBA-35S-SE-CFP and pBA-35S-PAG1-YFP were infiltrated separately or coinfiltrated into the leaves of four-week-old tobacco plants (N. benthamiana). The fluorescence resonance energy transfer assays were performed as previously described⁴⁷. The YFP and CFP signals were captured with an Olympus FV1000 confocal microscope with excitation wavelengths of 515 nm and 405 nm. ImageJ (v.1.52a) was used for normalization and analysis⁴⁷. For the PAG1 and SE localization assay, stable transgenic plants were imaged on a Nikon D-ECLIPSE C1si confocal laser scanning microscope.

Co-IP assay. For the Co-IP experiments with the transient expression system, all of the tested constructs were transformed into Agrobacterium strain ABI and then co-infiltrated into four-week-old leaves of N. benthamiana. Leaf samples were collected two days after agroinfiltration, and total protein extracts were prepared from 0.4 g of ground powder using 1.2 ml of IP buffer (40 mM Tris-HCl, pH 8.0, 100 mM NaCl, 1 mM EDTA, 1 mM dithiothreitol (DTT), 0.2% Triton X-100, 1 mM phenylmethyl sulfonyl fluoride (PMSF), 1% glycerol, 1 pellet per 12.5 ml Complete EDTA-free protease inhibitor (Roche), 50 µM MG132). The total protein extracts were then centrifuged twice for 15 min at 21,000 g at 4 °C. The final supernatants were immunoprecipitated with 3 µl of anti-SE antibody at 4 °C for 3 h. Then, 18 µl of magnetic Protein A beads that had been washed with IP buffer three times were added to the extracts at 4°C for an additional hour. The unspecific-bound proteins were removed by three consecutive washes with IP buffer. For RNaseA treatment, 0.05 mg ml⁻¹ RNaseA was added to the IP buffer during incubation. The beads were boiled with 2× SDS-loading buffer for the western blot analyses using an anti-SE antibody for SE IP proteins and an anti-YFP antibody for co-immunoprecipitates. For the Co-IP experiments with Arabidopsis plants, ten-day-old wild-type Col-0 and transgenic seedlings were used. The IP buffer and process were identical to the ones in the transient system. The beads were boiled with $2\times$ SDS-loading buffer for the western blot analyses using an anti-SE/anti-YFP antibody for IP proteins and two kinds of anti-ubiquitin antibody (Santa Cruz Biotechnology, sc8017; Agrisera, AS08307) for the detection of ubiquitin in the input and the immunoprecipitates.

RNA blot and western blot assays. Total RNA was extracted using TRI reagent (Sigma T9424) from either ten-day-old seedlings or three-week-old adult plants. The RNA blot hybridizations of low-molecular-weight RNAs (sRNA blot) and high-molecular-weight RNAs (northern blot) were performed as described previously²⁹. The probe for detecting SE transcript was labelled by $[\alpha^{-32}P]$ dCTP with Klenow fragment and PCR template of SE (1,405 to 2,082 nucleotides using the primers listed in Supplementary Table 1). The sRNA probes were labelled by [γ-32P] ATP with T4 PNK and 21-nucleotide DNA oligos that are complementary to the corresponding sRNAs (the primers are listed in Supplementary Table 1). Hybridization signals were detected with Typhoon FLA7000 (GE Healthcare). Western blot analysis was performed as previously described⁴⁴. The blots were detected with antibodies against FLAG (Sigma F1804), YFP (Roche 11814460001 and Agrisera AS15 2987), actin (Sigma A0480), histone 3 (Agrisera AS10 710), AGO1 (Agrisera AS09 527), SE (Agrisera AS09 532A), ubiquitin (Santa Cruz Biotechnology, sc8017; Agrisera AS08 307), HYL1 (from Seong Wook Yang's laboratory⁴⁸), DCL1 (Agrisera AS12 2102), His (Sigma H1029) and Myc (Sigma C3956). Secondary antibodies were goat-developed anti-rabbit (GE Healthcare, cat. no. NA934) and anti-mouse IgG (GE Healthcare, cat. no. NA931).

RT-PCR and qRT-PCR. Total RNA was extracted with the TRI Reagent (Sigma T9424) from three-week-old soil-grown plants, treated with DNase (Sigma AMPD1) to remove residue DNA and reverse transcribed by Superscript III reverse transcriptase (Invitrogen) using random primers. Quantitative PCR was performed with SYBR Green master mix (Bio-Rad). $EFI\alpha$ was included as an internal control for normalization. The primers used for PCR are listed in Supplementary Table 1.

SEC assays. SEC was performed as previously described with modifications¹⁷. Ten-day-old Col-0 and pag1-2 seedlings were harvested, ground to a fine powder in liquid nitrogen and mixed with 2 ml $\rm g^{-1}$ of extraction buffer (20 mM Tris-HCl, pH 7.5, 300 mM NaCl, 4 mM MgCl₂, 200 μM ZnCl₂, 0.1% Triton X-100, 1% glycerol, $4 \times$ EDTA-free protease inhibitor (Roche), 2 mM PMSF and 15 μ M MG132). The total protein extracts were centrifuged twice at 4°C for 15 min at 15,000 rpm. The supernatant was then filtered through a 0.2 μm filter. Next, the total protein extracts for each sample were loaded onto a Superdex 200 10/300 GL column (GE Healthcare) that was prewashed with a balance buffer (20 mM Tris-HCl, pH 7.5, 300 mM NaCl, 4 mM MgCl $_2$, 200 μ M ZnCl $_2$, 0.1% Triton X-100, 1% glycerol, 1/3× EDTA-free protease inhibitor (Roche), 0.5 mM PMSF and $15\,\mu\text{M}$ MG132). The running buffer contained 20 mM Tris-HCl, pH 7.5, 300 mM NaCl, 4 mM MgCl₂, 200 μM ZnCl₂, 0.1% Triton X-100, 1% glycerol, 1× EDTA-free protease inhibitor (Roche), 2 mM PMSF and 15 µM MG132. Fractions were collected for western blot analysis using an anti-SE antibody for SE. The Superdex 200 column was also calibrated by the gel filtration standard (Bio-Rad).

RNA and sRNA sequencing and bioinformatics. Total RNA was extracted with the TRI Reagent (Sigma T9424) from three-week-old soil-grown plants. The Illumina sequencing library preparation and analysis were performed as previously

described²⁵. The sRNA sequences from different samples were normalized with the number of residue rRNA reads with perfect genomic matches.

Affinity purification of 20S proteasomes. The 20S proteasome purification assays were performed as previously described^{6,33}. Briefly, ten-day-old pBA002a- P_{PAGI} -gPAGI-FM transgenic seedlings were used for affinity purification of the Arabidopsis proteasome. First, 5 g of seedlings were ground to a fine powder in liquid nitrogen and homogenized with 8 ml of extraction buffer (50 mM Tris-HCl, pH 7.5, 25 mM NaCl, 2 mM MgCl $_2$, 1 mM EDTA, 5% (v/v) glycerol and 2 mM PMSF). The total protein extracts were filtered through Miracloth (Calbiochem) and centrifuged twice at 4°C for 15 min at 15,000 rpm. The final supernatants were immunoprecipitated with the anti-FLAG M2 magnetic bead (Sigma M8823) at 4°C for 30 min; the beads were then washed three times with washing buffer (50 mM Tris-HCl, pH 7.5, 800 mM NaCl, 2 mM MgCl₂, 1 mM EDTA, 5% (v/v) glycerol and 2 mM PMSF) and eluted with 250 µl of extraction buffer containing 500 ng µl⁻¹ of the 3XFLAG peptide (DYKDDDDK) by 30 min rotation at 4°C. For 26 S proteasome purification, the extraction buffer was supplemented with 10 mM ATP, and the washing buffer was the same as the extraction buffer. The purified proteasomes were stored at −80 °C.

In vitro 20S proteasome-decay assay. The activity of the purified proteasome was first tested with the substrate succinyl-Leu-Leu-Val-Tyr-7-amido-4-methylcoumarin (Suc-LLVY-AMC) (Sigma S6510) as previously described 6,33 . 10 µl of the purified proteasome was incubated with 90 µl of reaction buffer (50 mM Tris-HCl, pH 7.5, 25 mM NaCl, 2 mM MgCl $_2$ 1 mM EDTA, 2 mM DTT, 5% glycerol and 50 µM Suc-LLVY-AMC substrate). The fluorescence reading of the released 7-amido-4-methylcoumarin (AMC) was monitored at the indicated times by fluorescence using 380 nm excitation and 440 nm emission wavelengths. The concentrations of proteasome and test proteins were estimated by the Bradford method 19 using bovine serum albumin as a standard.

The 20S proteasome-decay assays were performed on the basis of a previous protocol 35 . SE and HYL1 proteins were purified as described by previous work 17 . SE and HYL1 (150 nM) were incubated with purified 20S proteasome (10 nM) in a reaction mixture containing 50 mM Tris-HCl (pH 7.5) and 2% DMSO or 50 μ M MG132 (dissolved in 2% DMSO). The mixtures were then aliquoted into PCR tubes followed by incubation in a PCR machine (22 °C, lid 37 °C). The reaction was stopped by adding 2x SDS–PAGE loading buffer at the indicated times (0, 5, 10, 20 and 30 min), followed by western blot analysis using anti-SE and anti-HYL1 antibodies.

In vivo CHX-decay assay and chemical treatments. For the CHX-decay assay, wild-type Col-0, *pag1-2* and *35S-FM-SE* transgenic plants were germinated and grown on solid MS media for ten days before transfer to liquid MS medium supplemented with the indicated concentrations of MG132 (Calbiochem 474787), PYR-41 (Sigma N2915) and/or CHX (Sigma C1988) in each experiment. The samples were treated for 15 min under vacuum and then incubated at the room temperature for the indicated times (0, 1, 2, 4 and 6 h) before western blot analysis.

In vitro cell-free decay assay. The in vitro cell-free decay assay was carried out as previously described with modifications 30,32 . Ten-day-old seedlings of Col-0 and pag1-2 were harvested, ground to a fine powder in liquid nitrogen, mixed with twofold volume of lysis buffer (25 mM Tris-HCl, pH 7.5, 10 mM NaCl, 10 mM MgCl₂ and 10% glycerol) and incubated at 4 °C for 30 min. The total protein extracts of each sample were centrifuged twice at 4 °C for 10 min at 13,000 rpm and then were adjusted to equal concentrations with the lysis buffer. The final supernatant was supplemented with 0.5 mM CHX and 5 mM ATP, and the mixtures were then divided into two parts. One aliquot was added with $50\,\mu\text{M}$ MG132 or $50\,\mu\text{M}$ PYR-41 and the other with 2% DMSO as a control. The mixtures were then incubated at 22 °C for the indicated times (0, 10, 20, 30, 40, 50, 60, 120 and 240 min) described in each experiment before western blot analysis.

Nuclear-cytoplasmic fractionation assay. Three-week-old soil-grown plants were used for the nuclear-cytoplasmic fractionation experiment as previously described50. First, 0.5 g samples were ground to a fine powder in liquid nitrogen and mixed with two volumes of lysis buffer (20 mM Tris-HCl, pH 7.5, 20 mM KCl, 2 mM EDTA, 2.5 mM MgCl₂, 25% glycerol, 250 mM sucrose, 5 mM DTT and 1 pellet per 12.5 ml Complete EDTA-free protease inhibitor (Roche)). The samples were then filtered through two layers of Miracloth and centrifuged at 1,500 g for 10 min at 4 °C. After centrifugation, the supernatant and pellet were collected. The supernatant parts were then centrifuged again at 10,000 g for 10 min at 4 °C and collected for western blot analysis. The pellet parts were washed four times with nuclear resuspension buffer 1 (20 mM Tris-HCl, pH 7.4, 25% glycerol, 2.5 mM MgCl₂ and 0.2% Triton X-100). After washing, the pellet was resuspended with 500 ml of nuclear resuspension buffer 2 (20 mM Tris-HCl, pH 7.5, 0.25 M sucrose, 10 mM MgCl₂, 0.5% Triton X-100, 5 mM β-mercaptoethanol and 1 pellet per 12.5 ml Complete EDTA-free protease inhibitor (Roche)); then, 500 ml of nuclear resuspension buffer 3 (20 mM Tris-HCl, pH 7.5, 1.7 M sucrose, 10 mM MgCl₂, 0.5% Triton X-100, 5 mM β-mercaptoethanol and 1 pellet per 12.5 ml Complete EDTA-free protease inhibitor (Roche)) was carefully added on the top of samples,

and they were centrifuged at $16,000\,g$ for $45\,\text{min}$ at $4\,^{\circ}\text{C}$. The final pellet was resuspended in $400\,\text{ml}$ of lysis buffer and collected for western blot analysis. The quality of fractionation was validated with cytoplasmic and nuclear markers: Rubisco stained with Ponceau S and histone 3 detected by an anti-H3, respectively.

Reporting Summary. Further information on research design is available in the Nature Research Reporting Summary linked to this article.

Data availability

The RNA-seq and sRNA-seq data were deposited in the NCBI BioProject database with accession code PRJNA613247. All other data supporting the findings of the study are present in the main text and/or the Supplementary Information. Additional data related to this study are available from the corresponding authors upon request. Source data are provided with this paper.

Received: 17 September 2019; Accepted: 16 April 2020; Published online: 20 July 2020

References

- Collins, G. A. & Goldberg, A. L. The logic of the 26S proteasome. Cell 169, 792–806 (2017).
- Vierstra, R. D. The ubiquitin–26S proteasome system at the nexus of plant biology. Nat. Rev. Mol. Cell Biol. 10, 385–397 (2009).
- Groll, M. et al. Structure of 20S proteasome from yeast at 2.4 Å resolution. Nature 386, 463–471 (1997).
- Bard, J. A. M. et al. Structure and function of the 26S proteasome. Annu. Rev. Biochem. 87, 697–724 (2018).
- Dong, Y. et al. Cryo-EM structures and dynamics of substrate-engaged human 26S proteasome. Nature 565, 49–55 (2019).
- Book, A. J. et al. Affinity purification of the *Arabidopsis* 26 S proteasome reveals a diverse array of plant proteolytic complexes. *J. Biol. Chem.* 285, 25554–25569 (2010).
- Deshmukh, F. K., Yaffe, D., Olshina, M. A., Ben-Nissan, G. & Sharon, M. The contribution of the 20S proteasome to proteostasis. *Biomolecules* 9, E190 (2019).
- Asher, G., Reuven, N. & Shaul, Y. 20S proteasomes and protein degradation "by default". *Bioessays* 28, 844–849 (2006).
- Erales, J. & Coffino, P. Ubiquitin-independent proteasomal degradation. Biochim. Biophys. Acta 1843, 216–221 (2014).
- Grigg, S., Canales, C., Hay, A. & Tsiantis, M. SERRATE coordinates shoot meristem function and leaf axial patterning in *Arabidopsis. Nature* 437, 1022–1026 (2005).
- 11. Yang, S. S. et al. Accumulation of genome-specific transcripts, transcription factors and phytohormonal regulators during e arly stages of fiber cell development in allotetraploid cotton. *Plant J.* **47**, 761–775 (2006).
- Dong, Z., Han, M. & Fedoroff, N. The RNA-binding proteins HYL1 and SE promote accurate in vitro processing of pri-miRNA by DCL1. *Proc. Natl Acad. Sci. USA* 105, 9970–9975 (2008).
- 13. Iwata, Y., Takahashi, M., Fedoroff, N. V. & Hamdan, S. M. Dissecting the interactions of SERRATE with RNA and DICER-LIKE 1 in *Arabidopsis* microRNA precursor processing. *Nucleic Acids Res.* 41, 9129–9140 (2013).
- Machida, S., Chen, H. & Yuan, A. Molecular insights into miRNA processing by *Arabidopsis thaliana* SERRATE. *Nucleic Acids Res.* 39, 7828–7836 (2011).
- Yang, S. W. et al. Structure of Arabidopsis HYPONASTIC LEAVES1 and its molecular implications for miRNA processing. Structure 18, 594–605 (2010).
- Zhu, H. L. et al. Bidirectional processing of pri-miRNAs with branched terminal loops by *Arabidopsis* Dicer-like 1. *Nat. Struct. Mol. Biol.* 20, 1106–1115 (2013).
- Wang, Z. et al. SWI2/SNF2 ATPase CHR2 remodels pri-miRNAs via SE to impede miRNA production. *Nature* 557, 516–521 (2018).
- Gruber, J. J. et al. Ars2 links the nuclear cap-binding complex to RNA interference and cell proliferation. Cell 138, 328–339 (2009).
- Sabin, L. R. et al. Ars2 regulates both miRNA- and siRNA-dependent silencing and suppresses RNA virus infection in *Drosophila*. Cell 138, 340–351 (2009).
- Laubinger, S. et al. Dual roles of the nuclear cap-binding complex and SERRATE in pre mRNA splicing and microRNA processing in *Arabidopsis thaliana*. Proc. Natl Acad. Sci. USA 105, 8795–8800 (2008).
- Laubinger, S. et al. Global effects of the small RNA biogenesis machinery on the *Arabidopsis thaliana* transcriptome. *Proc. Natl Acad. Sci. USA* 107, 17466–17473 (2010).
- Gruber, J. J. et al. Ars2 promotes proper replication-dependent histone mRNA 3' end formation. Mol. Cell 45, 87–98 (2012).

- Hallais, M. et al. CBC-ARS2 stimulates 3'-end maturation of multiple RNA families and favors cap-proximal processing. *Nat. Struct. Mol. Biol.* 12, 1358–1366 (2013).
- Raczynska, K. D. et al. The SERRATE protein is involved in alternative splicing in Arabidopsis thaliana. Nucleic Acids Res. 42, 1224–1244 (2014).
- Ma, Z. et al. Arabidopsis Serrate coordinates histone methyltransferases ATXR5/6 and RNA processing factor RDR6 to regulate transposon expression. Dev. Cell 45, 769–784 (2018).
- Speth, C. et al. Arabidopsis RNA processing factor SERRATE regulates the transcription of intronless genes. eLife 7, e37078 (2018).
- Andreu-Agullo, C., Maurin, T., Thompson, C. B. & Lai, E. C. Ars2 maintains neural stem-cell identity through direct transcriptional activation of Sox2. *Nature* 481, 195–198 (2012).
- Schulze, W. M., Stein, F., Rettel, M., Nanao, M. & Cusack, S. Structural analysis of human ARS2 as a platform for co-transcriptional RNA sorting. *Nat. Commun.* 9, 1701 (2018).
- Zhang, X. R. et al. Cucumber mosaic virus-encoded 2b suppressor inhibits Arabidopsis Argonautel cleavage activity to counter plant defense. Genes Dev. 20, 3255–3268 (2006).
- Zhong, S. X. et al. Anaphase-promoting complex/cyclosome regulates RdDM activity by degrading DMS3 in *Arabidopsis. Proc. Natl Acad. Sci. USA* 116, 3899–3908 (2019).
- Zhang, Z. H. et al. KETCH1 imports HYL1 to nucleus for miRNA biogenesis in Arabidopsis. Proc. Natl Acad. Sci. USA 114, 4011–4016 (2017).
- Zhao, Q. et al. A plant-specific in vitro ubiquitination analysis system. Plant J. 74, 524–533 (2013).
- 33. Han, J. J. et al. The β 5 subunit is essential for intact 26S proteasome assembly to specifically promote plant autotrophic growth under salt stress. *New Phytol.* **221**, 1359–1368 (2019).
- 34. Prilusky, J. et al. FoldIndex: a simple tool to predict whether a given protein sequence is intrinsically unfolded. *Bioinformatics* 21, 3435–3438 (2005).
- Hsieh, L. S., Su, W. M., Han, G. S. & Carman, G. M. Phosphorylation regulates the ubiquitin-independent degradation of yeast Pah1 phosphatidate phosphatase by the 20S proteasome. *J. Biol. Chem.* 290, 11467–11478 (2015).
- Fang, Y. & Spector, D. L. Identification of nuclear dicing bodies containing proteins for microRNA biogenesis in living *Arabidopsis* plants. *Curr. Biol.* 17, 818–823 (2007)
- Fedorova, O. A. et al. Proteomic analysis of the 20S proteasome (PSMA3)-interacting proteins reveals a functional link between the proteasome and mRNA metabolism. *Biochem. Biophys. Res. Commun.* 416, 258–265 (2011).
- Ju, D. & Xie, Y. Proteasomal degradation of RPN4 via two distinct mechanisms, ubiquitin-dependent and -independent. J. Biol. Chem. 279, 23851–23854 (2004).
- Tofaris, G. K., Layfield, R. & Spillantini, M. G. α-Synuclein metabolism and aggregation is linked to ubiquitin-independent degradation by the proteasome. FEBS Lett. 509, 22–26 (2001).
- 40. $\dot{L}i$, X. et al. Ubiquitin-and ATP-independent proteolytic turnover of p21 by the REG γ -proteasome pathway. *Mol. Cell* **26**, 831–842 (2007).
- Tsvetkov, P., Reuven, N. & Shaul, Y. Ubiquitin-independent p53 proteasomal degradation. Cell Death Differ. 17, 103–108 (2010).
- Hwang, S. G. et al. Regulation of beta-catenin signaling and maintenance of chondrocyte differentiation by ubiquitin-independent proteasomal degradation of alpha-catenin. *J. Biol. Chem.* 280, 12758–12765 (2005).
- Zhang, X. R., Henriques, R., Lin, S. S., Niu, Q. W. & Chua, N. H. Agrobacterium-mediated transformation of *Arabidopsis thaliana* using the floral dip method. *Nat. Protoc.* 1, 641–646 (2006).
- Zhu, H. L. et al. Arabidopsis Argonaute10 specifically sequesters miR166/165 to regulate shoot apical meristem development. Cell 145, 242–256 (2011).
- 45. Zhang, Z. H. et al. RISC-interacting clearing 3'-5' exoribonucleases (RICEs) degrade uridylated cleavage fragments to maintain functional RISC in *Arabidopsis thaliana*. *eLife* **6**, e24466 (2017).
- 46. He, P., S, L. B. & Sheen, J. The use of protoplasts to study innate immune responses. *Methods Mol. Biol.* **354**, 1–9 (2007).
- Banerjee, S., Garcia, L. R. & Versaw, W. K. Quantitative imaging of FRET-based biosensors for cell- and organelle-specific analyses in plants. *Microsc. Microanal.* 22, 300–310 (2016).
- Cho, S. K., Chaabane, S. B., Shah, P., Poulsen, C. P. & Yang, S. W. COP1 E3 ligase protects HYL1 to retain microRNA biogenesis. *Nat. Commun.* 5, 5867 (2014).
- Bradford, M. M. A rapid and sensitive method for the quantitation of microgram quantities of protein utilizing the principle of protein-dye binding. *Anal. Biochem.* 72, 248–254 (1976).
- Wang, W. et al. An importin beta protein negatively regulates microRNA activity in Arabidopsis. Plant Cell 23, 3565–3576 (2011).

Acknowledgements

We thank Zhang lab members for careful proofreading of this manuscript. The work was supported by grants from the NIH (grant nos. GM132401 and GM127742), NSF (grant

no. MCB-1716243) and Welch Foundation (grant no. A-1973-20180324) to X.Z. Y.L., D.S., L.W. and X.Y. were supported by China Scholar Council fellowships.

Author contributions

X.Z. conceived the project. Z.W. and X.Z. designed the study. Y.L. and D.S. performed the experiments. Z.M. conducted the bioinformatics analysis. B.S., Y.N. and H.K. helped with the confocal experiments. K.Y., L.W., M.Z., S.Z., X.Y., J.H. and Q.X. provided the experimental materials and intellectual input. Y.L., D.S. and Z.W. analysed the data. Y.L. and X.Z. wrote the paper.

Competing interests

The authors declare no competing interests.

Additional information

Extended data is available for this paper at https://doi.org/10.1038/s41477-020-0721-4. **Supplementary information** is available for this paper at https://doi.org/10.1038/s41477-020-0721-4.

Correspondence and requests for materials should be addressed to Z.W. or X.Z.

Peer review information *Nature Plants* thanks Yijun Qi and the other, anonymous, reviewer(s) for their contribution to the peer review of this work.

Reprints and permissions information is available at www.nature.com/reprints.

Publisher's note Springer Nature remains neutral with regard to jurisdictional claims in published maps and institutional affiliations.

© The Author(s), under exclusive licence to Springer Nature Limited 2020